DEPARTMENT OF THE INTERIOR

U.S. GEOLOGICAL SURVEY

A Survey of Natural Fractures at the Hi Vista Site, Mojave Desert, California

by

James E. Springer and Mark J. Ader
U.S. Geological Survey

Open-File Report 87-24

Menlo Park, California

1987

CONTENTS

TABLES

FIGURES

UNITED STATES
DEPARTMENT OF THE INTERIOR
GEOLOGICAL SURVEY

A SURVEY OF NATURAL FRACTURES AT THE HI VISTA SITE, MOJAVE DESERT, CALIFORNIA

James E. Springer and Mark J. Ader

ABSTRACT

An array of five wells was drilled in Mesozoic granitic rock for hydrological and geophisical investigations at Hi Vista, California. A 592 m-deep well is located in the center of the array and four 183 m-deep wells were drilled 14 m from it in each of the cardinal directions. Two hundred seventy-seven fractures were seen in televiewer logs of the deep well and three significant fracture sets were identified; a north-striking high-angle set, a northeast-striking high-angle set, and a low-angle set that dips to the west-southwest. Each of the shallow wells contained some fractures within these sets; however the distributions of fracture orientations varied from well to well. These different fracture orientations may help to explain why water levels between wells vary by as much as 50 m.

When these fracture distributions are compared with those from three other deep holes in crystalline rock at Black Butte, Crystallaire, and Cajon Pass, a regional trend can be identified. Each of the wells has significant clustering associated with it. Two of the clusters identified at Hi Vista are well defined in more than one deep hole. Fracture frequency at Hi Vista increases with depth; that at Cajon Pass decreases with depth; and the fracture frequencies at Black Butte and Crystallaire show no strong systematic trend with depth.

INTRODUCTION

Natural fractures are one of the most important and least understood phenomena in rock mechanics. They exert a profound influece on ground water flow, heat flow, seismic velocity, anisotropy, and effective elastic moduli. Their genesis is related to the stresses that existed when they formed and their presence affects the way that the earth's crust responds to contemporary tectonic stresses. Knowing the fracture distribution at depth in the western Mojave desert is an important factor in understanding questions about local and regional hydrology (eg. Stierman, 1986), seismic wave propogation, stress variations in the crust (eg. Stock et al., 1986), and the relationship between

in-situ stress and heat flow (eg. Lachenbruch et al., 1986). The wells at Hi Vista, California provide an opportunity to analyze the fracture distribution at various depths and understand how it varies spacially over a small area. Other studies of fractures at depth have been done in the region (Seeburger and Zoback, 1982; Springer and Myren, 1985; Springer et al., 1986) and this paper compares the results of these investigations.

The Hi Vista site (fig. 1) is located on the northeast side of the town of Hi Vista, 50 km east of Lancaster and 32 km northeast of the San Andreas fault in the western Mojave Desert. The site was chosen for its location relative to the Fort Tejon-Palmdale segment of the San Andreas fault and because the low permeability crystalline rock at the site lends itself to both in-situ stress measurements and strain monitoring. An array of five wells was drilled at the site (fig. 2). The first hole, located in the center of the array was drilled to a depth of 592 m for the purpose of hydraulic fracturing stress measurements (McGarr et al., 1982). The hole is now being used to monitor secular changes in fluid pressure that reflect earth tides and may indicate precursors to earthquakes (Healy and Urban, 1985). The other four holes, designated as N-50, E-50, S-50, and W-50 were drilled to a depth of 183 m, and each is located 15 m from the deep hole. The purpose of these holes was to investigate the hydrologic regime and understand the communication of fluid between deep and shallow aquifers (Stierman and Healy, 1985).

Borehole televiewer (BHTV) logs were run in all five holes. The BHTV is an ultrasonic imaging device (Zemanek, et al., 1970) that produces a picture of the inside of the borehole. The logs were run in order to evaluate fractures and other discontinuities, investigate the condition of the wellbore, and to locate favorable intervals for geophysical measurements and instrumentation.

The purpose of this paper is to determine the distribution and characteristics of fractures in the five holes. A summary of the site geology is presented, followed by a brief discussion of the methods of logging and interpretation. Finally we present the results of the fracture analysis and discussion of the relationship between the fractures and ground water hydrology.

SITE GEOLOGY

The Hi Vista site is located on a gently northwest-sloping pediplane in the high desert. Elevation of the site is about 915 m and the elevation difference between the tops of the wells is less than 1 m. The nearest topographic high lies 7 km to the southwest and has a peak elevation of 1,098 m. The rock encountered in the well is a regionally extensive granite of late Mesozoic age (Ross, 1972).

The hydrologic conditions at Hi Vista are very complex. The amount of time necessary for the water level to reach equilibrium after drilling varied considerably between wells with the deep

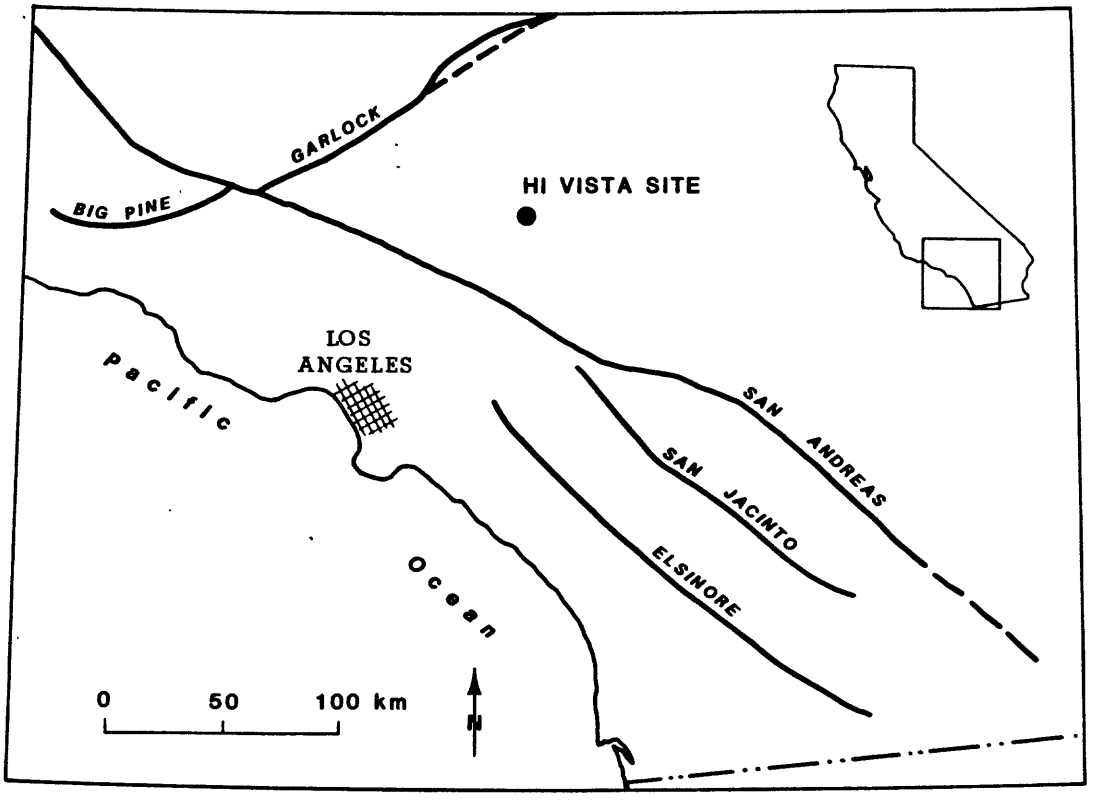

Fig. 1. Location map of the Hi Vista site.

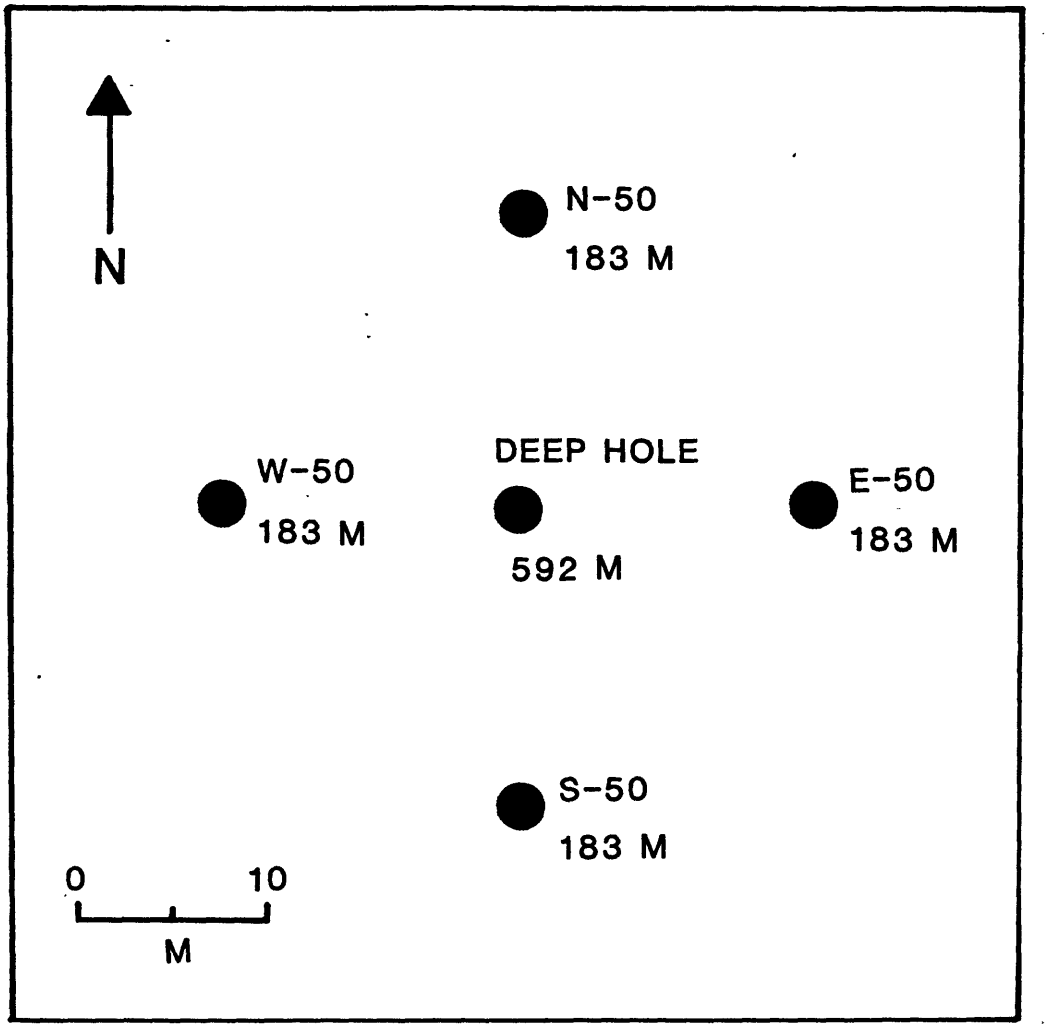

Fig. 2. Layout of the Hi Vista wells.

well taking several tens of minutes and S-50 taking almost seven months (Healy and Urban, 1985). The water level in the deep hole was reported to be 117 m by Stierman and Healy (1985) and the hole was later cemented to 480 m to isolate deep fractures from shallow ones. Water level determinations in wells N-50, E-50, S-50, and W-50 are shown in Table 1. In some cases, water levels were measured directly with a wireline-operated conductivity bridge that was lowered into the hole (D. Stierman, personal communication). In other cases the water level was determined from the televiewer. (A televiewer signal can only be detected if it propogates through a liquid medium so the water level is taken as the depth that the return signal disappears). After drilling, water rose quickly in most of the holes to static water levels that varied by as much as 50 m between holes (Stierman and Healy, 1985).

TABLE 1

Water Level Determinations in the Hi Vista Holes

N-50

Date	Depth	Source
2/14/83	113.45 m	Televiewer
8/23/85	109.36 m	Direct measurement

E-50

Date	Depth	Source
2/16/83	65.91 m	Televiewer
3/22/85	62.13 m	Televiewer
8/23/85	61.13 m	Direct measurement

S-50

Date	Depth	Source
3/23/85	111.86 m	Televiewer
8/23/85	112.41 m	Direct measurement

W-50

Date	Depth	Source
2/15/83	109.39 m	Televiewer
3/24/85	101.71 m	Televiewer
8/23/85	106.1 m	Direct measurement

ANALYSIS OF FRACTURES

Borehole Televiewer

Fractures were identified and characterized using the BHTV which consists of a centralized logging sonde with a rotating lead metheniobate crystal piezoelectric transducer. The trans-

ducer rotates three times per second and emits and receives an average of 600 pulses of 1.3 MHz acoustic energy per revolution. A flux-gate magnetometer in the tool triggers on magnetic north and keys the orientation of the transducer. The transducer describes a spiral as the tool is logged up the hole at 1.5 m/ min.

The return signal is sent through a four conductor wireline to the surface for processing. The amplitude of the signal is output as a function of brightness on the z-axis of a three axis oscilloscope. Each horizontal sweep of the scope starts at magnetic north on the left edge of the field of view and moves to east, south, west, and then north again as the transducer rotates clockwise. The scope display is photographed as successive sweeps move up the scope. The resulting log is an acoustic picture of the inside of the borehole as if it were split down the middle and laid flat (fig. 3). The brightness is a function of the smoothness of the well bore and the acoustic impedence contrast between the borehole wall and the fluid in the hole.

Planar discontinuities, such as fractures, which cross the borehole show up as dark sinusoidal traces on the log. The dip direction of a fracture is the azimuthal location of the trough of the sinusoid. The strike is 90 degrees to the dip direction. The dip angle is related to the height, h of the sinusoid, and the diameter, d of the hole by the relationship:

$$\text{dip} = \tan^{-1} h/d$$

(Zemanek, et al., 1970). There is a horizontal exaggeration of the immage that is a function of the hole size and the logging speed. For a typical 15 cm diameter hole that is logged at 1.5 m/ min, the horizontal exaggeration is about 8:1. For this reason, computed orientations of low-angle fractures are less accurate than those of high-angle fractures.

Results

Fracture Orientations:

Fracture poles from the deep hole were plotted on a lower hemisphere, equal area projection and contoured using a statistical method developed by Kamb (1959). This method contours the probability that the observed orientation could not have resulted from a random sample of a population that lacks preferred orientation. The contour interval is 2σ , where σ is the standard deviation of the total number of points in a given area under random sampling. The counting area A is selected so that the expected frequency E for no preferred orientation is 3σ . When the observed density is two or three times this value, the preferred orientation is likely to be significant.

Two hundred seventy-seven fractures were identified in the deep hole. The distribution of orientations of these fractures is shown on the lower hemisphere contoured pole plot in fig. 4. There is considerable dispersion, however three prominent sets

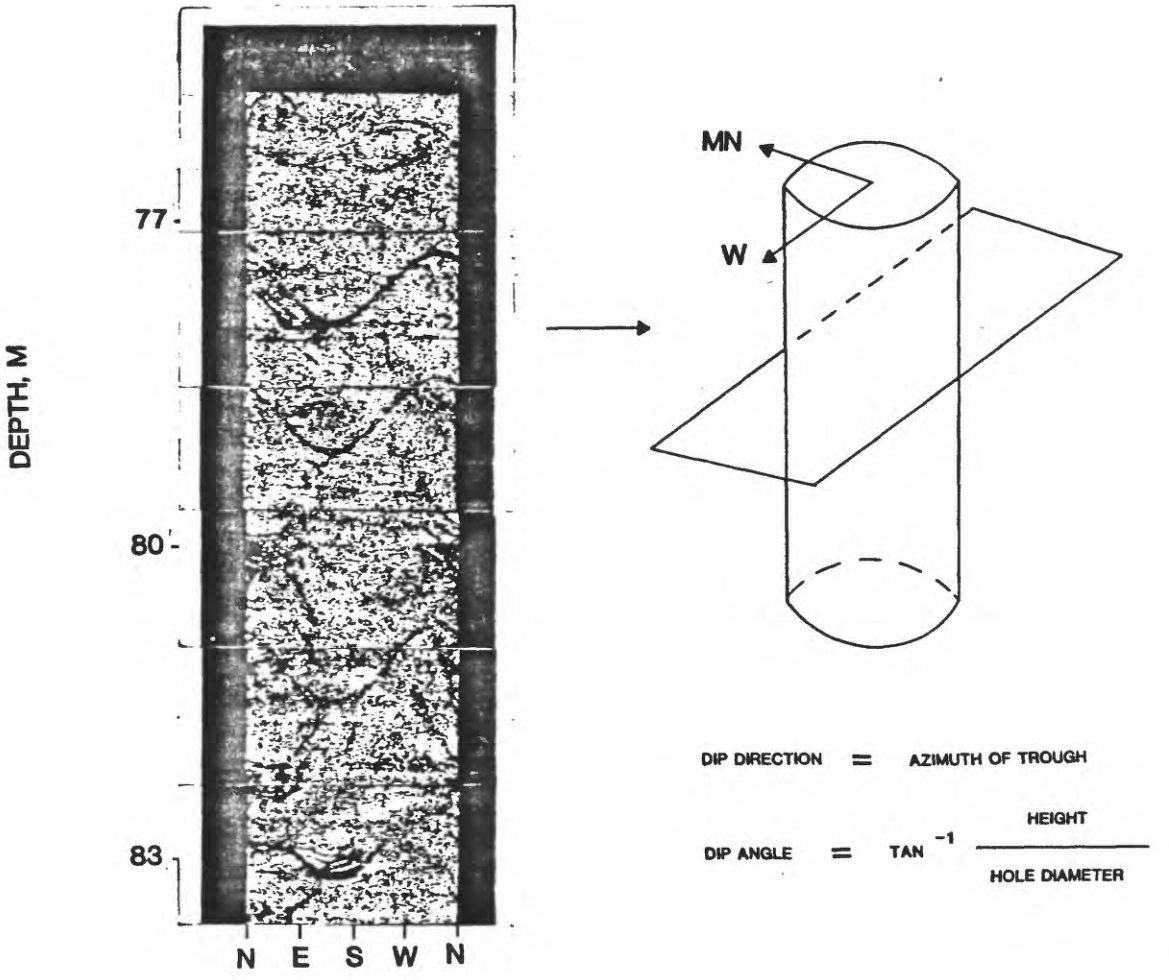

Fig. 3. Example of part of a televiewer log.

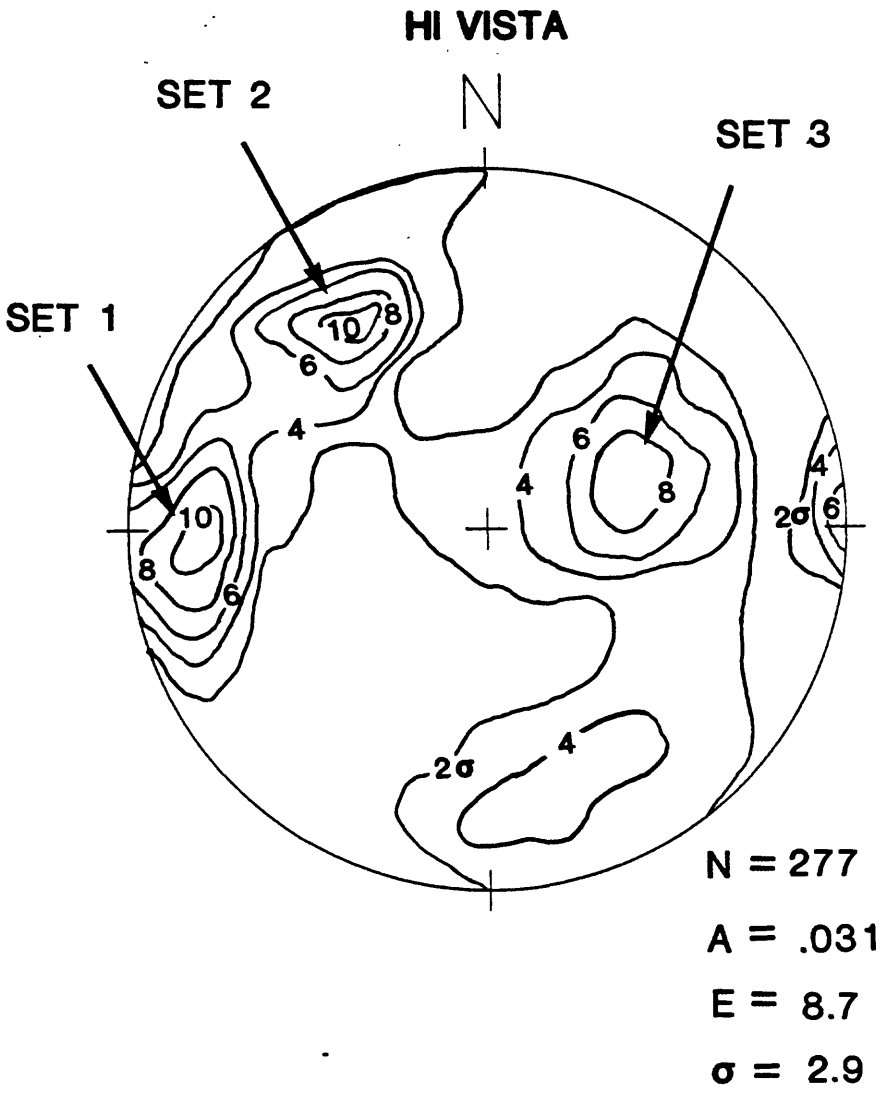

Fig. 4. Contoured lower hemisphere equal area plot of poles to 277 fractures in the deep well. The statistical contouring method is that used by Kamb (1959). The contour interval is 2σ where σ is the standard deviation of the total number of points in a given area under random sampling. The area A is selected so that the expected frequency for no preferred orientation is 3σ. When the observed density is two or three times this value, a preferred orientation is likely to be significant.

are evident; a high-angle, north-striking set (set 1), a high-angle, northeast-striking set (set 2), and a low-angle set that dips to the west-southwest (set 3). The lower hemisphere pole plots shown in fig. 5 represent the actual observations with 5a representing all observations and 5b, c, d, and e representing observations at various depth intervals. The north-striking set (set 1) is present throughout the hole (fig. 5b, c, d, and e). Set 2 and set 3 become stronger with depth and are prominent below 336 m (fig. 5d and e). A large amount of dispersion exists in this data set.

The total number of fractures in each of the other wells was considerably smaller. This was because the wells were shallower and therefore sampled a smaller volume of the rock mass. N-50 had 29 fractures (fig. 6); E-50 had 67 fractures (fig. 7); S-50 had 25 fractures (fig. 8); and W-50 had 76 fractures (fig. 9). The few fractures in N-50 show a tendency toward a preferred orientation with a north to north-northeast-striking high-angle cluster (fig. 6), similar to set 2 found in the deep hole (fig. 4). The plot of E-50 (fig. 7) contains sets 1 and 2 as well as some scattered sub-horizontal fractures. Fractures in S-50 are nearly all high-angle with a mean dip angle of 74 degrees. The orientation distribution in this hole (fig. 8) is different from the rest of the holes and while the strikes of the fractures are spread out over a wide range of azimuth, most of them dip away from the other wells. W-50 contains several fractures that are close to set 1 seen in the deep hole, N-50, and E-50. The predominant cluster, however, is a high-angle northwest-striking set that is not prominent in any of the other holes (fig. 9).

It can be seen from figs. 5 through 9 that, while there are similarities in orientations between the wells, the most noteworthy feature is the differences betweem wells. Although the small sample sizes in these wells render the statistical significance of these differences questionable, the observed differences may begin to explain why the wells have such different hydrologic properties. The occurence of different fracture orientation distributions over a small area was also observed in two holes drilled 300 m apart near Black Butte (Springer and Myren, 1985).

Fracture Frequency:

Fracture frequencies were plotted as a function of depth in figs. 10 through 13. Frequencies on the left half of these figures are taken from raw fracture counts. Since fractures oriented at a low angle to the well bore axis have a lower probability of intersecting the hole, the frequencies on the right half of the figures were corrected by adjusting the fracture count using:

$$C_{corr.} = 1/\cos(\alpha)$$

where $C_{corr.}$ is the corrected fracture count and α is the angle between the fracture and the plane normal to the borehole axis. (For a vertical well, α is equal to the dip angle). The uncorrected fracture frequency is representative of what is intersecting the well. The corrected frequency is representative

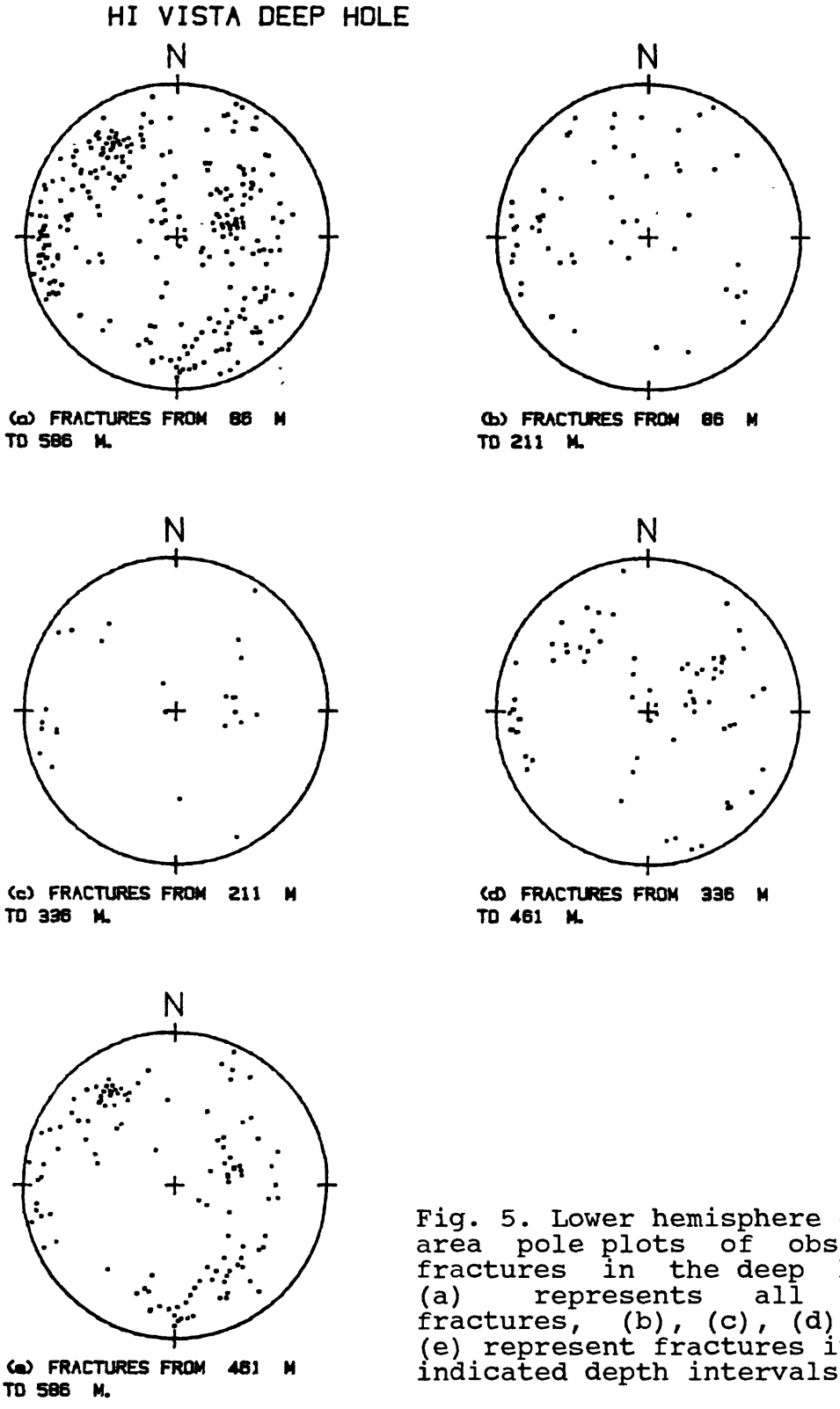

Fig. 5. Lower hemisphere equal area pole plots of observed fractures in the deep hole. (a) represents all the fractures, (b), (c), (d), and (e) represent fractures in the indicated depth intervals.

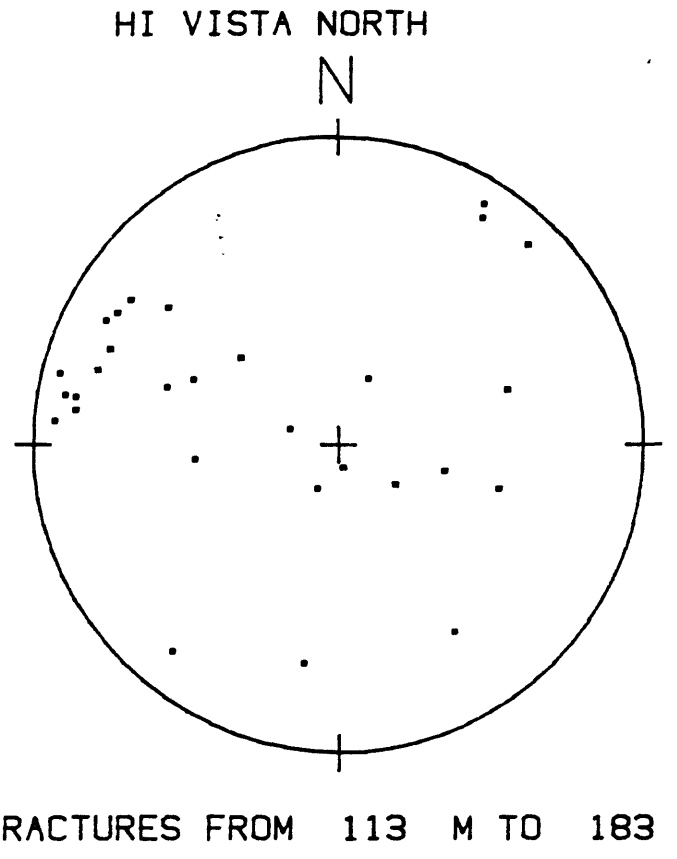

Fig. 6. Lower hemisphere equal area pole plot of the 29 observed fractures in the N-50 well.

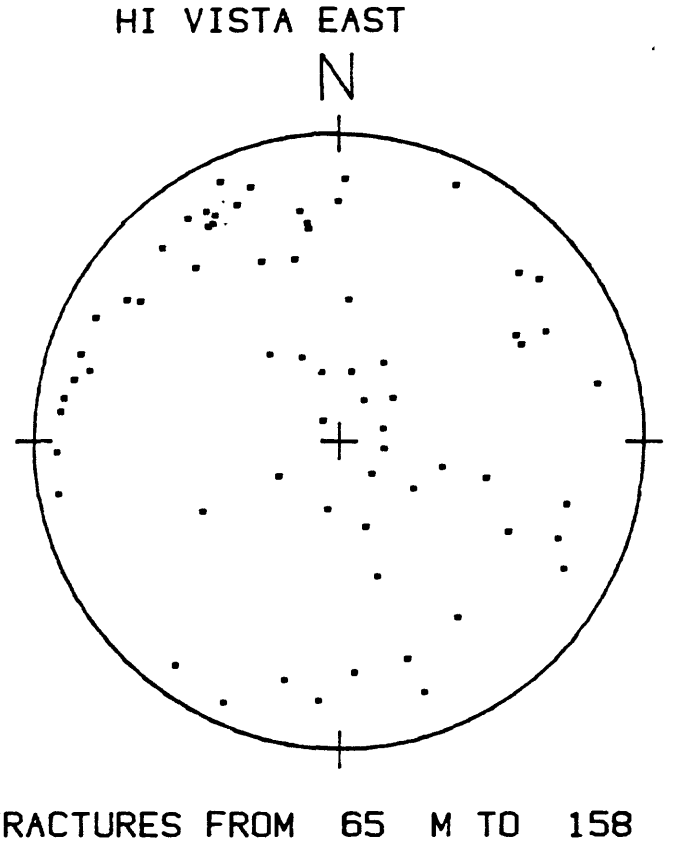

Fig. 7. Lower hemisphere equal area pole plot of the 67 observed fractures in the E-50 well.

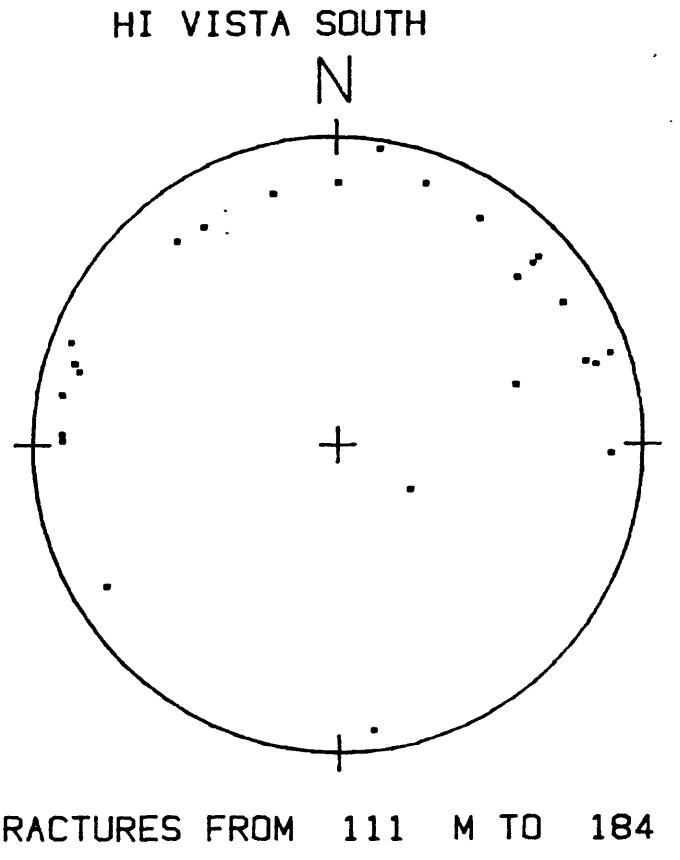

Fig. 8. Lower hemisphere equal area pole plot of the 25 observed fractures in the S-50 well.

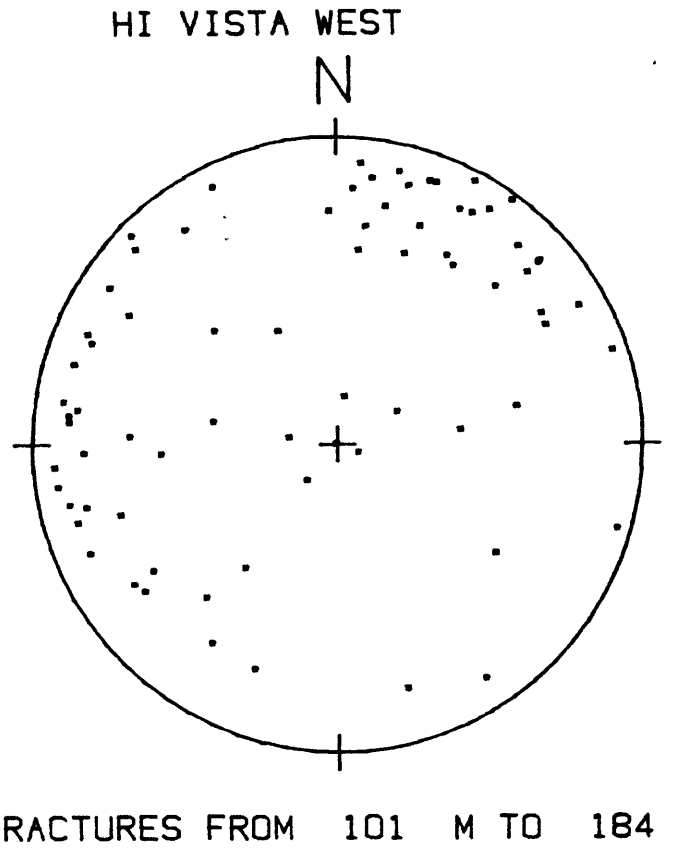

Fig. 9. Lower hemisphere equal area pole plot of the 76 observed fractures in the W-50 well.

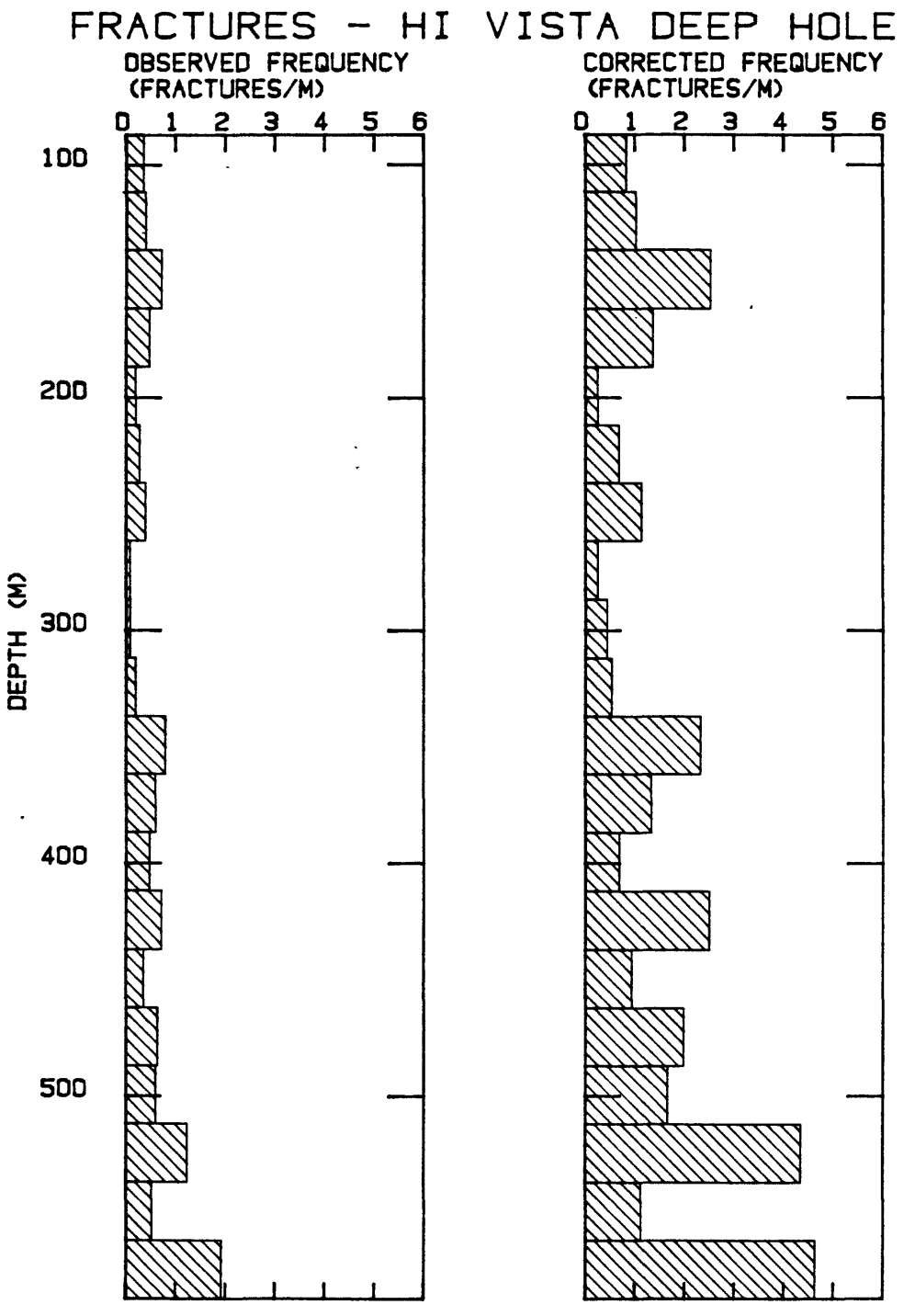

Fig. 10. Fracture frequency as a function of depth in the deep well. The graph on the left shows the observed frequency and the graph on the right shows the frequency after correcting for the orientation of the fractures with respect to the orientation of the hole.

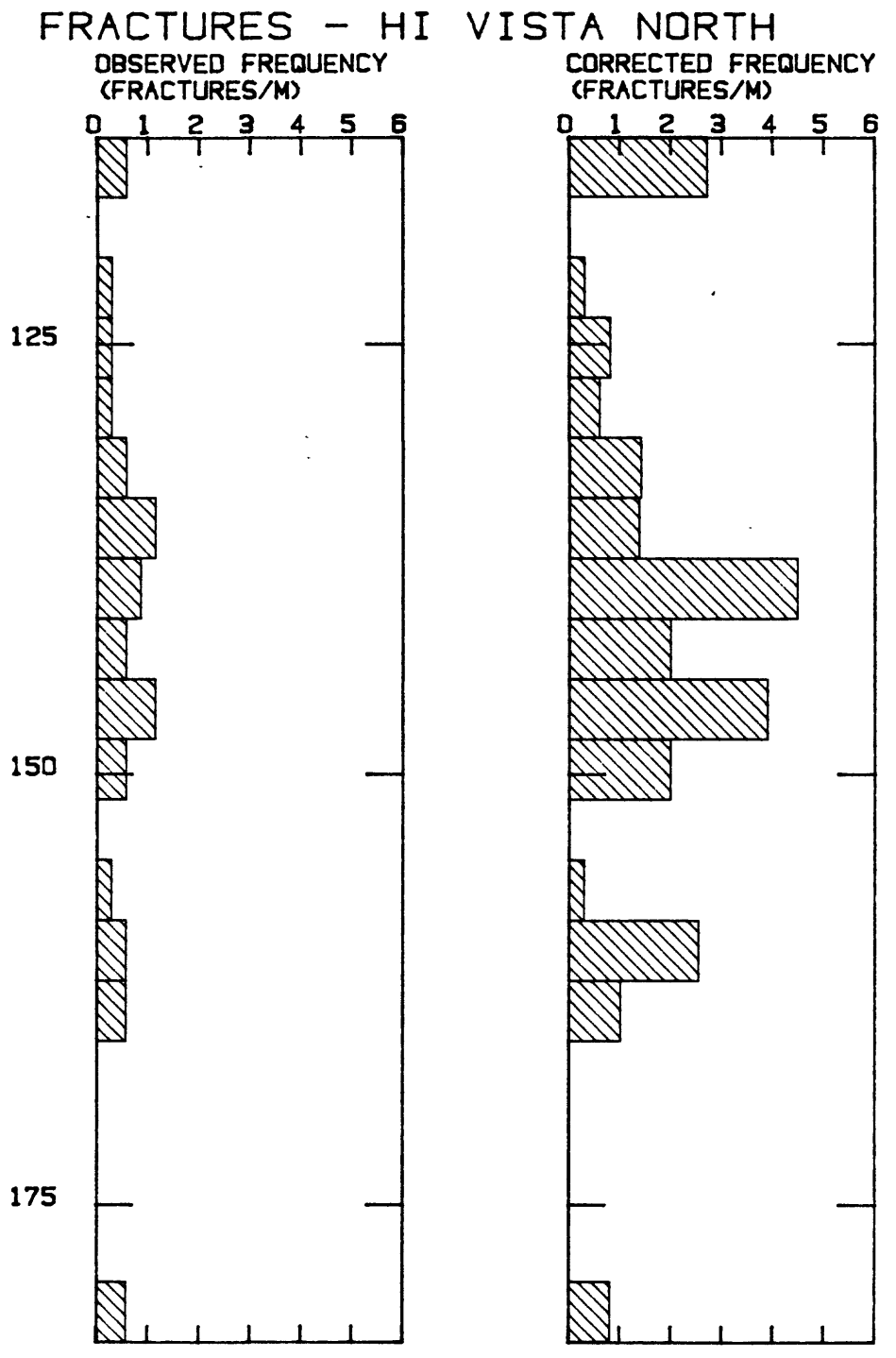

Fig. 11. Observed and corrected fracture frequency as a function of depth in the N-50 hole.

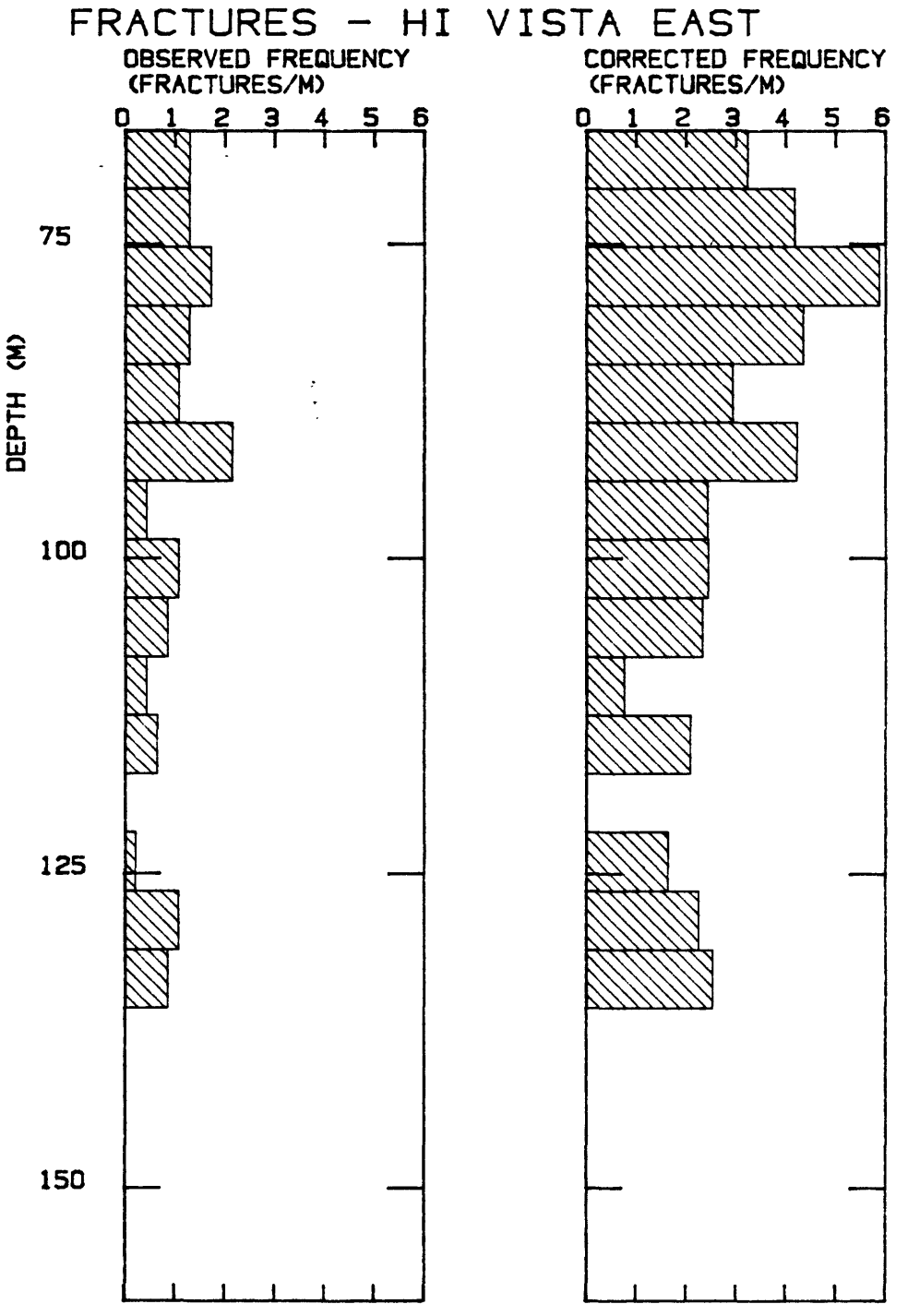

Fig. 12. Observed and corrected fracture frequency as a function of depth in the E-50 hole.

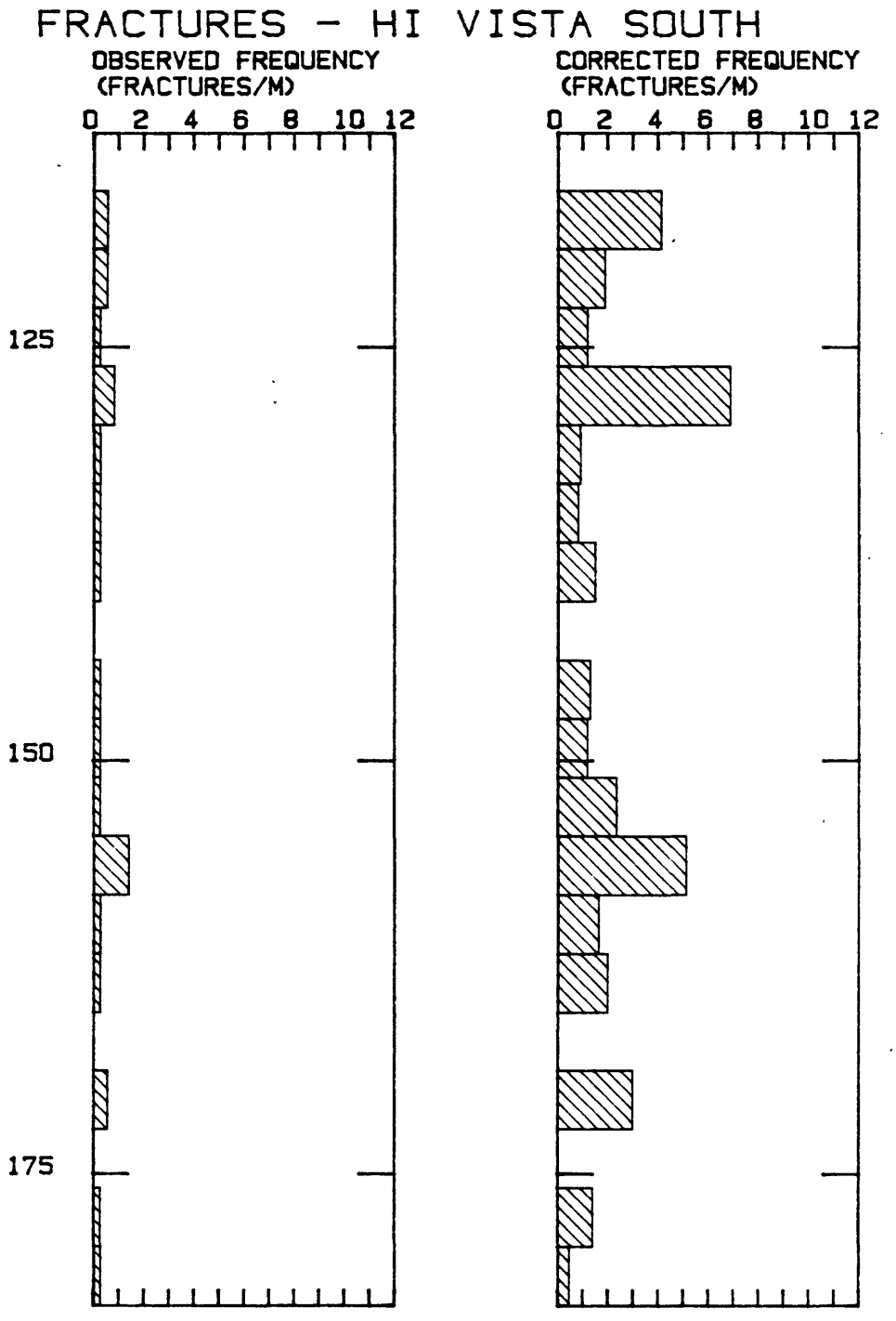

Fig. 13. Observed and corrected fracture frequency as a function of depth in the S-50 hole.

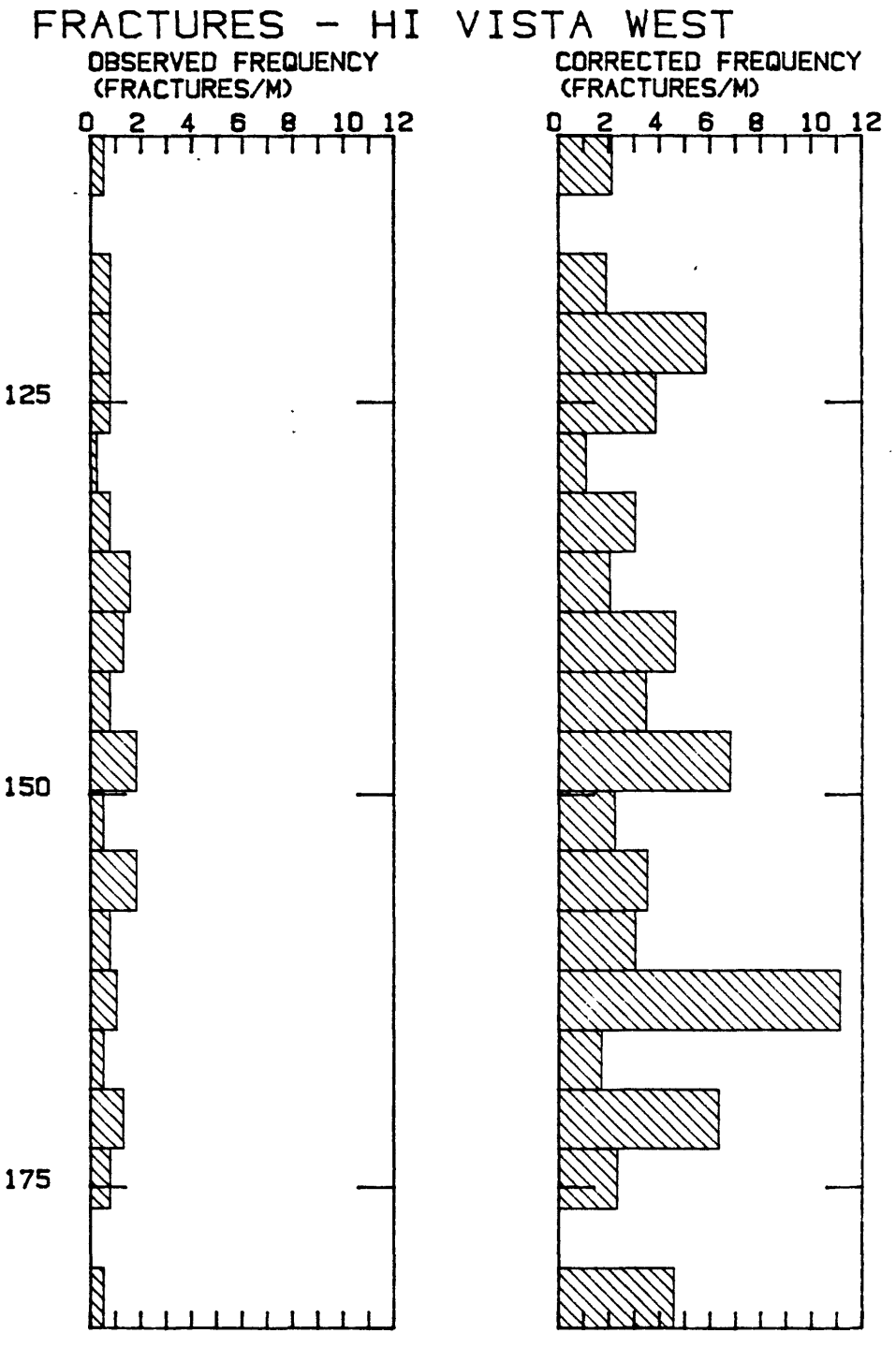

Fig. 14. Observed and corrected fracture frequency as a function of depth in the W-50 hole.

of the degree of fracturing that exists in the rock mass.

The average frequency in the deep hole is 0.55 fractures/m and it shows a general increase with depth, as shown in fig. 10. The corrected frequency shows a more pronounced increase with depth because high-angle fractures, which are given more weight, become relatively more frequent near the bottom of the hole. The density of fracturing varies from hole to hole, however the four shallow holes are sampling a much smaller part of the rock mass and their frequency distributions may be less significant than the deep hole. The average frequency in N-50 is 0.41 fractures/m with the highest frequencies being between 135 and 150 m (fig. 11). The east hole has an average frequency 0.72 fractures/m with a general decrease in frequency with depth (fig. 12). The average frequency in S-50 is 0.34 fractures/m and a general trend with depth is not obvious (fig. 13). The average frequency in W-50 is 0.84 fractures/m and a slight general increase in frequency with depth is only obvious with the corrected frequencies (fig. 14).

Comparison with Regional Fracture Patterns:

Studies of fractures in other wells in the Mojave desert region have been done by Seeburger and Zoback (1982), Springer and Myren (1985), and Springer et al. (1986). When Seeburger and Zoback (1982) did their work, the only deep well in the region was the 869 m-deep one at Crystallaire, designated as XTLR (fig. 15). They compared the distributions of fractures in this well with those from three shallower wells and found the orientations to be significantly different in each of the wells. Springer and Myren (1985) studied fractures in the 650 m-deep Black Butte hydrofrac hole (fig. 15) and a shallow hole drilled 300 m away from it. They found substantial differences in fracture orientations between these two holes. Springer et al. (1986) analyzed the fractures in a deep well at Cajon Pass which now has a depth of 1.8 km. They found the fracture frequency to be substantially less in this hole than it was in the other deep holes in the region.

A summary of the fracture orientations in each of the deep holes in the region is shown in fig. 15. Each hole has some significant preferred orientations. Set 1 can be seen clearly in the Black Butte hole. The Crystallaire hole has a more disperse main cluster whos dip is tilted slightly west of set 1. Set 2 is close to the only cluster in the Cajon Pass hole. Set 3 is poorly defined in Black Butte and Cajon Pass, but lies whithin the 6 sigma contour at Crystallaire. The observed fracture frequencies for each of these holes are shown in fig. 16. The frequency increases with depth in the Hi Vista hole and tends to decrease with depth in the Cajon Pass hole. The XTLR and Black Butte holes show no obvious trend in frequency with depth.

Fig. 15. Comparison of the orientation distribution of fractures in each of the deep holes from the Mojave region. Data for the XTLR hole is from Seeburger and Zoback (1982); data for the Black Butte hole is from Springer and Myren (1985); data for the Cajon Pass hole is from Springer et al. (1986); and data for the Hi Vista hole is from this study.

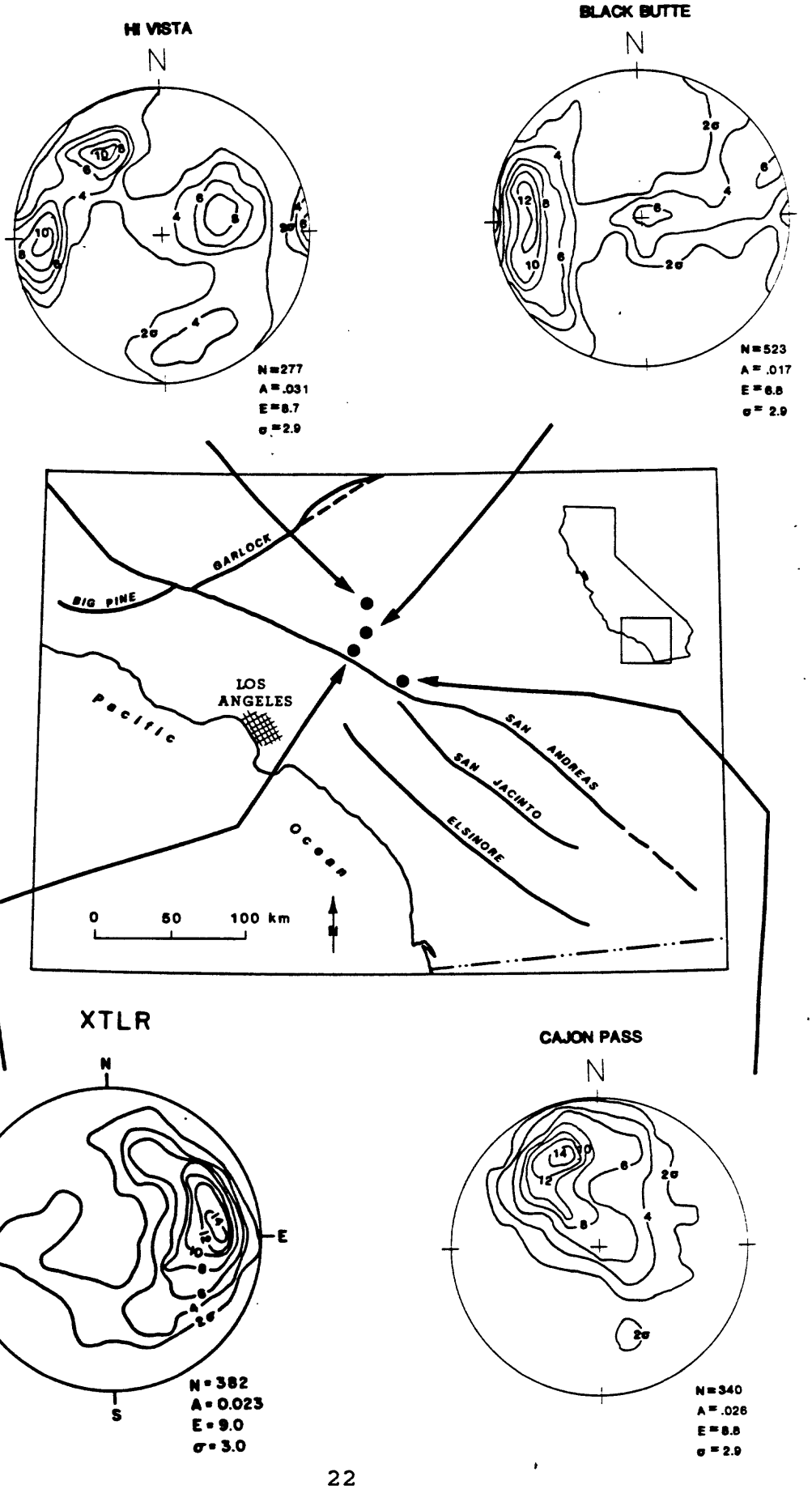
HI VISTA
N
N=277
A=.031
E=8.7
σ=2.9
BLACK BUTTE
N
N=523
A=.017
E=6.8
σ=2.9
BARLOCK
BIG PINE
LOS ANGELES
Pacific
Ocean
SAN ANDREAS
SAN JACINTO
ELSINORE
0 50 100 km
XTLR
N
W
E
S
N=382
A=0.023
E=9.0
σ=3.0
CAJON PASS
N
N=340
A=.026
E=8.8
σ=2.9

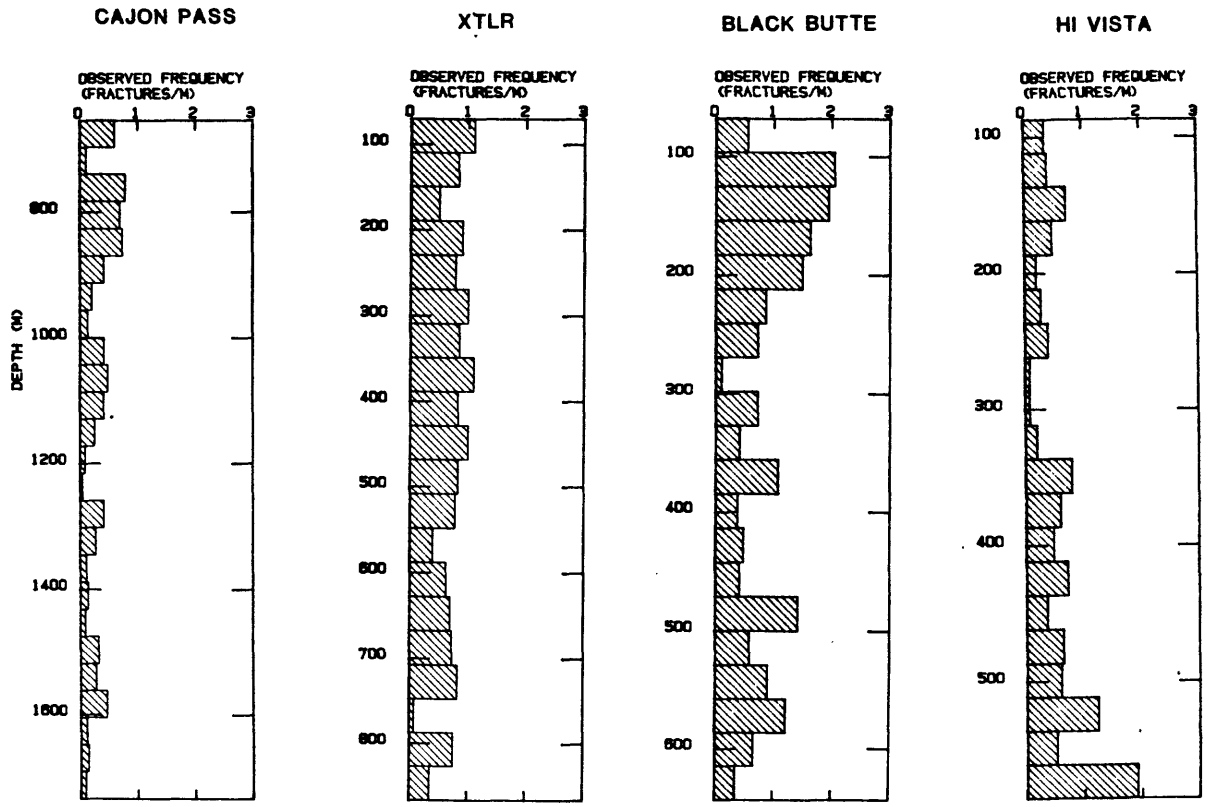

Fig. 16. Comparison of the observed fracture frequencies as a function of depth in the deep holes in the western Mojave region.

SUMMARY

Three sets of fractures with significant preferred orientations were identified from 277 fractures in the Hi Vista deep hole. Set 1 is high-angle and strikes to the north, set 2 is a northeast-striking high-angle set, and set 3 is low-angle and dips to the west-southwest. The fracture orientations observed in the other four wells are somewhat different and while this difference may not be statistically significant, it may have important implications on the hydrologic conditions at the site.

The distribution of fracture orientations is significantly different in all the deep wells drilled in crystalline rock in the region, however, two of the three clusters are well developed in more than one hole. This indicates that there is a regional trend of fracture orientations at depth.

The fracture frequency at Hi Vista increases with depth. In the deep hole at Cajon Pass, it decreases with depth. In the deep holes at Black Butte and Crystallaire, there is no obvious trend in fracture frequency with depth.

REFERENCES

Healy, J.H. and Urban, T.C., 1985, In-situ fluid-pressure measurements for earthquake prediction: an example from a deep well at Hi Vista, California: PAGEOPH, v.122, pp.255-279.

Kamb, W.B., 1959, Ice petrofabric observations from Blue Glacier, Washington, in relation to theory and experiment: Journal of Geophysical Research, v.64, no.11, pp.1891-1909.

Lachenbruch, A.H., Sass, J.H., Moses, T.H., Jr., and Galanis, S.P., Jr., 1986, Thermal studies at the Cajon Pass borehole: EOS, Transactions, American Geophysical Union, v.67, no.16, p.379.

McGarr, A., Zoback, M.D., and Hanks, T.C., 1982, Implications of an elastic analysis of in-situ stress measurements near the San Andreas fault: Journal of Geophysical Research, v.87, no.B9, pp.7797-7806.

Ross, D.C., 1972, Petrographic and chemical reconnaissance study of some granitic and gneissic rocks near the San Andreas fault from Bodega Head to Cajon Pass, California: U.S. Geological Survey, Professional Paper 698, 92p.

Springer, J.E., Barton, C., and Zoback, M.D., 1986, Natural fracture distribution and drilling-induced borehole elongation in the Cajon Pass well, California: EOS, Transactions, American Geophysical Union, v.67, no. 16, p.380.

Springer, J.E. and Myren, G.D., 1985, Geologic data report on the Black Butte hydrofrac hole, western San Bernardino County, California: U.S.G.S. Open-file Report 85-214, 25p.

Stierman, D.J., 1986, Effective stress and the water table in fractured granitic rock: EOS, Transactions, American

Geophysical Union, v.67, no. 16, p.373.
Stierman, D.J. and Healy, J.H., 1985, A study of depth of weathering and its relationship to the mechanical properties of near-surface rocks in the Mojave Desert: PAGEOPH, v.122, pp.425-439.
Stock, J.M., Healy, J.H., and Svitek, J.F., 1986, Hydraulic fracturing stress measurements at Black Butte, Mojave desert, CA: EOS, Transactions, American Geophysical Union, v.67, no.16, p.382.
Zemanek, J., Glenn, E.E., Norton, L.J., and Caldwell, R.L., 1970, Formation evaluation by inspection with the borehole televiewer: Geophysics, v.35, no.2, pp.254-269.

APPENDIX

Tables of Fractures Encountered in the Hi Vista Holes

The depth of each fracture is taken as the midpoint between the highest and lowest points of intersection with the borehole. The orientations are given as dip angle and azimuth of dip (dip direction).

HI VISTA DEEP HOLE

DEPTH	DIP	AZIM.	DEPTH	DIP	AZIM.
104.57	68.6	340.5	432.50	59.6	117.9
104.85	72.6	311.6	432.80	69.3	135.7
105.00	62.4	299.2	434.63	46.1	280.0
105.15	51.9	303.4	434.91	25.3	255.3
105.38	60.0	303.4	435.98	48.6	278.6
105.44	51.9	286.9	440.55	33.5	13.4
107.62	67.3	38.2	442.53	43.4	127.5
110.62	65.6	94.5	449.30	74.0	69.8
110.90	62.6	100.0	452.29	79.7	89.0
113.95	66.6	177.0	453.11	25.3	245.7
122.87	80.3	79.4	457.13	50.9	234.7
124.20	68.2	227.8	459.39	80.9	109.6
131.81	42.6	201.7	460.00	46.1	231.9
132.11	71.7	164.6	461.80	33.5	262.1
133.36	15.5	293.8	464.73	75.9	98.6
133.86	15.5	122.0	467.65	52.9	278.6
133.79	52.3	113.8	468.57	62.1	145.4
135.41	61.6	196.2	468.81	46.1	175.6
135.59	75.6	203.1	469.79	70.0	148.1
137.06	84.2	207.2	470.64	59.6	126.1
141.31	52.3	159.1	470.88	60.9	252.5
143.33	39.8	205.8	473.81	78.7	91.8
143.83	75.6	86.3	474.91	73.2	137.1
146.65	55.8	83.5	474.88	64.3	18.9
147.09	61.4	98.6	475.82	81.2	79.4
148.29	81.2	65.7	476.28	70.6	124.7
149.40	80.0	148.1	481.86	80.0	82.1
152.45	63.8	161.8	482.23	72.2	116.5
153.75	74.1	142.6	482.59	52.9	333.6
153.86	73.7	141.2	484.97	60.9	332.2
154.59	24.8	241.5	488.54	37.1	258.0
155.65	61.4	355.6	489.76	33.5	296.5
156.97	32.4	178.3	496.71	37.1	226.4
157.64	77.0	93.1	497.20	58.1	299.2
159.22	80.0	98.6	498.11	64.3	123.4
159.54	69.9	50.5	499.45	43.4	105.5
160.56	71.1	50.5	502.50	68.6	106.9
162.05	42.6	71.2	505.21	50.9	311.6
164.81	59.9	101.4	505.27	33.5	253.9
166.10	50.3	144.0	506.28	74.8	64.3
167.15	42.8	76.6	506.37	68.6	337.7
167.84	64.2	113.8	508.84	80.6	82.1
168.12	60.9	93.1	509.39	46.1	111.0
169.31	77.7	69.8	509.76	59.6	160.5
170.45	75.8	94.5	510.64	84.5	204.4
171.00	81.6	104.1	513.90	43.4	138.5
174.53	78.8	82.1	514.30	60.9	144.0
175.67	15.3	42.3	515.43	78.7	76.6
177.21	50.3	73.9	517.04	43.4	134.4
193.27	52.3	225.1	517.20	58.1	138.5
196.39	10.4	145.4	518.84	62.1	148.1
201.43	19.9	82.1	519.09	72.7	76.6
202.57	44.9	170.1	519.57	84.5	64.3
208.18	28.9	137.1	519.39	75.2	130.2
212.02	36.5	280.0	520.09	20.7	152.2
220.26	48.0	357.0	520.88	56.5	270.4
222.12	82.5	72.5	521.19	67.1	145.4
229.60	55.6	133.0	521.59	65.3	148.1
229.60	55.6	133.0	521.95	70.6	141.2
232.49	60.2	142.6	523.66	29.6	267.6
236.52	15.4	156.3	524.76	50.9	227.8

239.18	80.7	123.4	525.43	82.7	111.0
239.90	81.2	333.6	525.49	33.5	255.3
253.43	32.6	271.8	526.68	85.9	98.6
253.70	44.9	273.1	527.04	29.6	259.4
254.08	32.2	258.0	527.74	86.3	75.3
254.11	74.1	90.4	528.11	59.6	148.1
254.27	28.3	286.9	529.27	37.1	258.0
254.78	28.7	255.3	530.55	20.7	249.8
256.19	5.2	80.8	530.76	37.1	253.9
259.63	78.2	65.7	531.04	56.5	229.2
263.96	51.9	222.3	532.71	54.8	259.4
285.45	77.6	82.1	533.20	75.2	215.4
294.42	83.0	214.1	536.01	72.7	10.7
306.80	67.9	80.8	536.31	68.6	358.3
320.37	68.0	79.4	536.62	75.9	351.5
321.04	74.2	127.5	540.55	50.9	13.4
331.19	76.9	84.9	542.35	29.6	262.2
333.69	33.5	258.0	542.90	73.2	207.2
335.03	46.1	231.9	541.59	67.1	208.6
338.45	76.3	216.8	543.90	43.4	204.4
337.53	20.7	317.1	544.12	73.6	201.7
338.23	59.6	262.2	548.23	37.1	262.2
338.54	25.5	259.4	548.45	52.9	241.5
339.30	78.5	82.1	552.10	76.2	357.0
339.33	45.9	242.9	552.41	40.4	313.0
343.66	43.4	238.8	552.87	56.5	150.9
343.81	77.6	90.4	554.27	64.3	139.9
345.82	79.3	82.1	557.32	54.8	142.6
348.84	79.8	82.1	564.76	15.8	302.0
352.44	68.6	318.5	565.34	66.2	354.2
352.50	72.2	318.5	565.52	62.1	137.1
352.68	71.5	319.9	565.85	56.5	337.7
352.84	76.6	90.4	565.85	60.9	150.8
353.26	75.7	307.5	567.77	76.5	93.1
353.84	40.0	244.3	569.09	78.1	113.8
355.98	5.4	343.2	569.51	68.6	6.6
358.08	25.3	270.4	569.33	78.5	321.2
360.88	75.1	80.8	570.73	58.1	348.7
361.80	43.2	282.8	570.76	56.5	326.7
362.50	72.6	86.3	571.19	20.7	302.0
365.03	73.6	86.3	572.74	58.1	277.3
365.46	20.7	260.8	572.90	59.6	307.5
365.61	50.9	16.2	573.35	65.3	148.1
365.88	70.6	67.0	574.48	58.1	329.5
366.37	76.5	94.5	574.51	56.5	321.2
366.59	73.7	296.5	574.60	60.9	13.4
367.44	29.0	219.6	575.00	59.6	38.2
369.24	67.1	259.4	574.94	60.9	304.7
370.12	25.3	12.1	575.37	76.5	354.2
370.70	10.7	133.0	575.67	77.8	358.3
372.01	5.4	286.9	575.79	62.1	138.5
373.93	50.9	236.0	575.67	81.2	359.7
381.46	54.8	126.1	576.43	69.3	321.2
381.98	66.9	149.5	576.77	48.6	325.4
388.57	56.3	160.5	577.01	59.6	319.9
388.72	60.7	153.6	577.29	67.9	333.6
396.52	52.9	145.4	577.80	59.6	16.2
397.13	45.5	145.4	578.23	74.0	359.7
397.53	28.7	166.0	578.35	62.1	351.5
398.51	20.7	159.1	578.20	33.5	244.3
400.34	65.3	124.7	578.69	48.6	337.7
403.08	10.7	188.0	579.24	70.0	2.5
405.37	33.5	233.3	580.12	54.8	317.1
408.11	37.1	233.3	580.67	70.0	2.5
408.35	5.4	234.7	580.73	52.9	150.9
408.69	33.3	220.9	580.85	70.6	335.0

412.77	81.9	170.1	580.85	71.7	10.7
414.18	45.9	134.4	581.62	54.8	344.6
417.65	50.7	133.0	581.80	29.6	247.0
419.39	48.6	237.4	581.89	63.3	145.4
420.27	58.1	128.9	581.83	54.8	116.5
420.37	69.3	229.2	582.35	65.3	167.3
420.70	64.3	237.4	583.35	65.3	142.6
422.16	76.8	64.3	584.48	33.5	225.1
425.49	84.0	337.7	585.03	56.5	153.6
425.98	74.4	351.5	585.82	33.5	233.3
427.26	84.0	341.8			
429.85	76.2	80.8			

HI VISTA NORTH

DEPTH	DIP	AZIM.	DEPTH	DIP	AZIM.
114.15	79.4	100.1	145.44	48.9	108.2
116.42	75.6	100.1	145.63	70.8	124.6
122.43	19.0	206.4	145.91	59.8	128.7
124.57	69.2	112.3	147.82	81.9	94.6
130.14	61.4	327.8	149.27	72.1	120.5
131.17	75.2	97.3	150.29	74.3	117.8
133.72	6.5	345.5	157.31	12.9	23.7
134.42	19.0	304.6	161.05	82.7	104.1
134.86	29.8	284.1	160.78	12.9	106.9
136.27	34.5	131.4	162.21	45.9	285.5
136.41	42.5	113.7	162.42	61.4	8.7
139.62	79.0	224.1	179.88	48.9	252.8
139.77	80.7	211.9	179.85	38.8	83.7
140.23	76.4	213.2			
144.04	70.8	106.9			

HI VISTA EAST

DEPTH	DIP	AZIM.	DEPTH	DIP	AZIM.
66.07	41.6	284.1	91.43	60.6	172.0
67.45	77.3	116.6	91.63	18.4	232.9
69.22	18.4	58.4	92.10	37.8	184.4
70.00	77.6	102.7	92.22	18.4	191.4
70.62	62.1	140.1	92.49	73.8	181.7
70.57	37.8	343.7	93.31	23.9	156.7
72.64	74.7	149.8	94.93	77.6	116.6
73.47	70.2	148.4	98.46	81.3	87.5
73.86	73.8	137.4	99.98	65.8	242.6
74.04	68.6	12.7	99.83	41.6	62.6
74.28	75.6	340.9	100.78	71.5	123.5
75.22	64.6	356.1	101.06	72.2	151.2
76.80	82.3	79.2	102.73	29.0	284.1
77.50	12.5	255.0	104.18	67.7	124.9
78.09	23.9	342.3	105.00	53.1	156.7
78.59	81.5	155.4	106.28	77.6	108.3
78.95	76.0	160.9	106.64	57.2	239.8
79.38	76.0	145.7	110.40	50.7	166.4
79.63	6.3	141.5	108.91	59.0	325.7
79.92	53.1	298.0	113.73	73.3	105.5
80.20	80.4	95.8	114.94	70.2	149.8
80.42	12.5	280.0	116.39	72.2	156.7
81.98	76.0	257.8	123.95	82.5	23.8
81.86	12.5	314.6	128.58	80.7	205.2
84.45	66.8	285.5	128.27	12.5	213.5
84.59	79.6	36.3	128.45	18.4	166.4
85.26	29.0	141.5	128.66	23.9	210.7
85.55	63.4	342.3	128.83	23.9	302.1
85.54	59.0	172.0	131.79	73.8	299.4
86.94	67.7	293.8	132.23	73.3	231.5
87.70	79.8	98.6	132.49	69.4	227.4
90.45	64.6	170.6	134.11	57.2	242.6
90.30	18.4	8.6			
90.55	73.8	4.4			

HI VISTA SOUTH

DEPTH	DIP	AZIM.	DEPTH	DIP	AZIM.
115.58	78.7	90.7	155.95	76.5	238.5
116.90	84.0	251.9	156.23	76.1	227.7
119.31	72.6	141.8	156.22	23.1	301.6
121.30	72.6	166.0	156.93	75.0	251.9
125.08	76.1	105.5	157.35	78.0	253.3
127.91	78.5	106.9	159.27	80.1	100.1
128.73	86.4	188.8	164.21	81.9	110.9
128.89	73.6	180.7	168.82	79.4	272.1
132.84	71.5	148.5	169.24	78.9	92.1
133.41	69.4	227.7	178.93	78.5	199.5
140.39	79.2	227.7	180.69	52.0	251.9
144.30	77.4	58.5			
148.39	76.1	213.0			

HI VISTA WEST

DEPTH	DIP	AZIM.	DEPTH	DIP	AZIM.
103.02	81.3	81.1	145.58	12.5	97.4
103.14	78.4	77.1	146.38	55.3	200.2
103.51	77.3	73.0	146.52	60.4	211.1
104.02	73.3	75.7	147.29	78.6	124.5
105.71	62.1	55.4	148.19	77.3	66.3
105.78	63.4	71.7	148.79	67.7	52.7
106.34	33.7	152.9	149.41	80.2	213.8
106.77	74.3	97.4	149.26	75.2	208.4
106.98	67.7	240.8	151.34	69.4	55.4
107.22	81.6	154.2	152.45	79.8	133.9
107.79	55.3	40.5	153.65	68.4	238.1
108.21	77.0	96.0	154.01	33.7	263.9
109.12	73.8	144.8	154.18	50.7	258.4
117.83	48.0	86.6	154.88	45.0	132.6
118.48	41.6	36.5	155.68	67.7	192.1
119.27	76.7	94.7	156.37	62.1	226.0
121.09	85.7	286.9	157.46	72.7	228.7
121.31	79.6	327.5	157.32	53.1	186.7
121.30	71.5	87.9	157.44	64.6	201.6
124.63	66.8	20.2	160.73	80.1	201.6
124.65	64.6	178.6	161.88	87.5	216.5
125.49	84.1	135.3	162.45	86.2	208.4
127.63	76.0	188.1	162.85	71.7	184.0
131.20	78.3	106.9	163.95	18.4	242.2
131.74	75.2	112.3	165.48	12.5	39.2
132.34	68.1	121.7	167.86	79.4	98.7
135.02	6.3	290.9	169.29	80.5	240.8
135.10	12.5	189.4	170.15	60.6	188.1
135.28	0.0	196.2	171.91	76.0	196.2
136.30	33.7	100.1	172.09	80.0	193.5
136.82	57.2	92.0	172.21	80.5	185.4
137.36	53.1	304.5	174.31	77.6	113.6
138.41	76.7	223.2	174.33	0.0	194.8
138.60	77.6	228.7	175.70	71.5	343.7
141.08	58.8	213.8	181.15	85.1	251.7
141.43	65.6	32.4	182.55	79.8	200.2
141.84	76.2	211.1			
143.30	78.5	228.7			